MOTOROLA SOLUTIONS

COMPUTATIONAL EME COMPLIANCE ASSESSMENT OF THE XPR SERIES MODEL PMUD2567B MOBILE RADIO.

October 28, 2015

William Elliott, Giorgi Bit-Babik, Ph.D., and Antonio Faraone, Ph.D.
Motorola Solutions EME Research Lab, Plantation, Florida

Introduction

This report summarizes the computational [numerical modeling] analysis performed to document compliance of the XPR Series Model Number PMUD2567B Mobile Radio and vehicle-mounted antennas with the Federal Communications Commission (FCC) and Industry Canada (IC) guidelines for human exposure to radio frequency (RF) emissions. The radio operates in the 136 - 174 MHz frequency band.

This computational analysis supplements the measurements conducted to evaluate the compliance of the exposure from this mobile radio with respect to applicable *maximum permissible exposure* (MPE) limits. All test conditions (10 in total) that did not conform with applicable MPE limits were analyzed to determine whether those conditions complied with the *specific absorption rate* (SAR) limits for general public exposure (1.6 W/kg averaged over 1 gram of tissue and 0.08 W/kg averaged over the whole body) set forth in FCC guidelines, which are based on the IEEE C95.1-1999 standard [1]. The same test conditions were also analyzed to determine compliance with the SAR limits set forth in the ICNIRP [3] guidelines and IEEE Std. C95.1-2005 standard [4] (2.0 W/kg averaged over 10 gram of tissue and 0.08 W/kg averaged over the whole body). In total 20 independent simulations have been performed addressing exposure of passenger to the VHF mobile radio with trunk-mount antennas.

For all simulations a commercial code based on Finite-Difference-Time-Domain (FDTD) methodology was employed to carry out the computational analysis. It is well established and recognized within the scientific community that SAR is the primary dosimetric quantity used to evaluate the human body's absorption of RF energy and that MPE limits are in fact derived from

SAR. Accordingly, the SAR computations provide a scientifically valid and more relevant estimate of human exposure to RF energy.

Method

The simulation code employed is XFDTD™ v7.3.1, by Remcom Inc., State College, PA. This computational suite provides means to simulate the heterogeneous full human body model defined according to the draft IEC/IEEE 62704-2 standard and derived from the so-called Visible Human [2], discretized in 3 mm voxels. The draft IEC/IEEE 62704-2 standard dielectric properties of 39 body tissues are automatically assigned by XFDTD™ at any specific frequency. The "seated" man model was obtained from the standing model by modifying the articulation angles at the hips and the knees. Details of the computational method and model are provided in the Appendix to this report.

The car model has been imported into XFDTD™ from the CAD file of a sedan car having dimensions 4.98 m (L) x 1.85 m (W) x 1.18 m (H), and discretized with the minimum resolution of 3 mm and the maximum resolution of 9 mm. The Figure 1 below show both the CAD model and the photo of the actual car This CAD model has been incorporated into the IEC/IEEE 62704-2 draft standard.

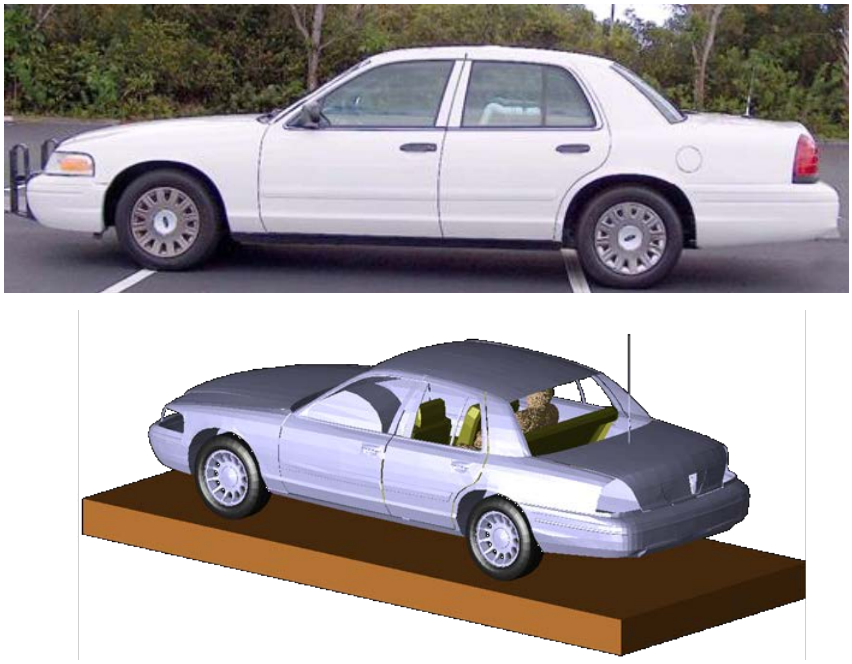

Figure 1: The photo picture of the car used in field measurements and the corresponding CAD model used in simulations

For bystander exposure, the antenna position is in the center of the trunk, so as to replicate the experimental conditions used in MPE measurements. Figure 2 shows some of the the XFDTD™ computational models used for bystander exposure.

For passenger exposure, the antenna position is on the trunk and the distance of trunk mounted antenna from the passenger head when the passenger is located in the center of the back seat was set at 85 cm, to replicate the experimental conditions used in MPE measurements. Figure 3 shows some of the XFDTD™ computational models used for passenger exposure to trunk mounted antennas

According to the IEC/IEEE 62704-2 draft standard (June 1, 2015) for exposure simulations from vehicle mount antennas the lossy dielectric slab with 30 cm thickness, dielectric constant of 8 and conductivity of 0.01 S/m has been introduced in the computational model to properly account for the effect of the ground (pavement) on exposure.

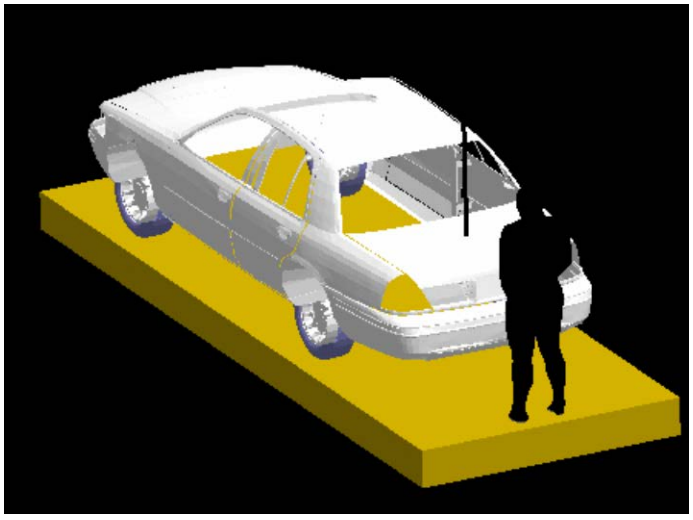

Figure 2: Bystander model exposed to a trunk-mount antenna: Bystander is located at the back, on the side or at the corner of the car replicating the measurement conditions. The antenna is mounted in the center of the trunk. The dielectric slab under the car is introduced to model the ground (pavement) effect on exposure.

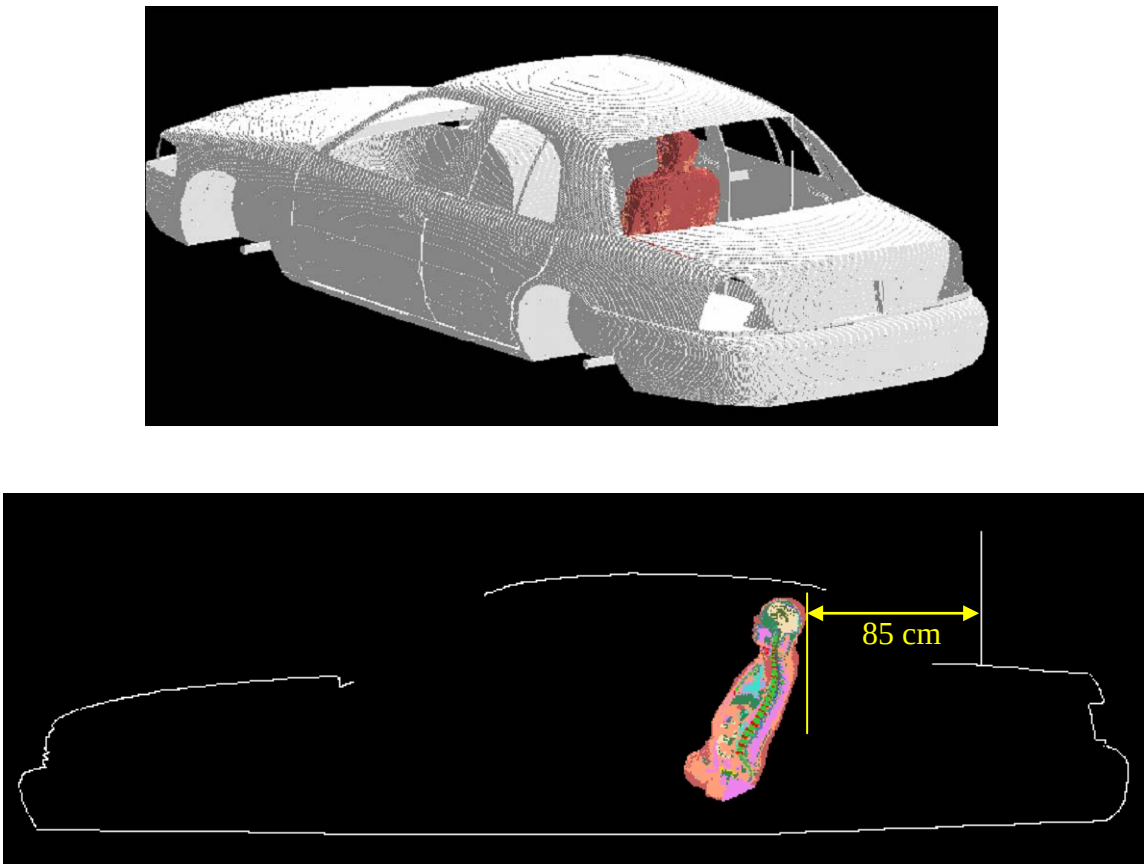

Figure 3: Passenger model exposed to a trunk-mount antenna: XFDTD geometry.
The antenna is mounted at 85 cm from the passenger located in the center of the back seat.

The computational code employs a time-harmonic excitation to produce a steady state electromagnetic field in the exposed body. Subsequently, the corresponding SAR distribution is automatically processed in order to determine the whole-body, 1-g, and 10-g average SAR. The maximum average output power from mobile radio antenna is 54 W. Since the ohmic losses in the cable and in the car materials, as well as the mismatch losses at the antenna feed-point, are neglected, and source-based time averaging (50% talk time) is employed, all computational results are normalized to half of it, i.e., 27 W average net output power.

Results of SAR computations for car passengers and bystanders

The test conditions requiring SAR computations are summarized in Table II, together with the antenna data, the SAR results, and power density (P.D.) as obtained from the measurements in the corresponding test conditions. The conditions are for antennas mounted on the trunk. The

antenna length in Table I includes the 1.8 cm magnetic mount base used in measurements to position the antenna on the vehicle. The same length was used in simulation model.

The passenger is located in the center or on the side of the rear seat. The passenger model is surrounded by air, as the seat, which is made out of poorly conductive fabrics, is not included in the computational model.

The bystander is located at the measurement distance from the transmit antenna as described in the original report and is assessed separately for front and back exposure.

All the transmit frequency, antenna length, and passenger location combinations reported in Table I have been simulated individually.

Table I: Results of the SAR computations for passenger exposure (50% talk-time).

Mount location	Antenna Kit #	Antenna length (cm)	Freq [MHz]	P.D. (mw/cm^2)	Exposure location	SAR [W/kg]		
						1-g	10-g	WB
Trunk	HAD4022A (132-174MHz)	120.1	143.9875	0.15	Back Center	0.443	0.282	0.0184
					Back Side	0.157	0.104	0.0112
		115.6	150.8	0.13	Back Center	0.286	0.177	0.0127
					Back Side	0.147	0.077	0.0080
		104.5	158.3	0.33	Back Center	0.335	0.201	0.0147
					Back Side	0.224	0.157	0.0121
		98.3	165.9875	0.56	Back Center	0.398	0.246	0.0162
					Back Side	0.251	0.225	0.0115
		91.7	173.4	0.44	Back Center	0.380	0.234	0.0171
					Back Side	0.306	0.191	0.0136
				0.14	Bystander 0 deg Front	0.156	0.101	0.0088
					Bystander 0 deg Rear	0.277	0.144	0.0067
				0.16	Bystander 45 deg Front	0.299	0.166	0.0094
					Bystander 45 deg Rear	0.310	0.180	0.0088
				0.15	Bystander 90 deg Front	0.316	0.203	0.0136
					Bystander 90 deg Rear	0.594	0.309	0.0141
Roof	HAD4006A (136-144MHz)	53.8	140.0125	0.23	Back Center	0.484	0.312	0.0197
					Back Side	0.325	0.188	0.0179
Roof	RAD4226A (136-144MHz)	52.2	140.0125	0.22	Back Center	0.480	0.309	0.0195
					Back Side	0.319	0.184	0.0175

SAR computational result adjustment to account for variations in the human body model

Peak spatial-average and whole-body average exposure varies from person to person due to physical and anatomical differences. As a result, adjustment factors to account for these variations have been determined by IEEE/IEC 62704-2 computational study [5].

To demonstrate compliance to the applicable limits, the computational results reported in Table I must be adjusted by the interpolated adjustment factors from the following tables found in draft IEEE/IEC 62704-2 (June 2015)

Table II: Peak spatial-average SAR adjustment factors for the passenger model and trunk mount antenna.

Frequency, MHz	Trunk mount antenna			
	Back seat, centre		Back seat, side	
	1-g	10-g	1-g	10-g
33	1.0	1.2	1.0	1.0
80	1.0	1.0	1.0	1.0
150	1.9	2.0	4.2	4.4
450	2.4	2.4	2.0	2.3
800	1.0	1.0	1.4	1.2
1000	1.3	1.1	1.0	1.0

Table III: Whole-body average SAR adjustment factors for the passenger and trunk mount antennas

Frequency, MHz	Passenger location in the vehicle	
	Back seat, centre	Back seat, side
33	1.0	1.0
80	1.4	1.0
150	2.4	3.0
450	2.8	2.6
800	2.2	1.9
1000	1.9	1.7

Table IV: Whole-body average SAR adjustment factors for the bystander and trunk mount antennas

Frequency, MHz	Bystander distance from the trunk mount antenna			
	80 cm	100 cm	120 cm	> 130 cm
30	1.0	1.0	1.0	1.0
50	1.3	1.3	1.4	1.4
75	1.7	2.0	2.2	2.3
100	2.5	2.5	2.5	3.5
150	1.9	1.9	2.5	4.5
300	2.1	2.6	2.6	2.6
450	1.4	1.3	1.5	2.0
800	1.0	1.0	1.0	1.0
1000	1.0	1.0	1.0	1.0

Table V: Peak spatial-average SAR adjustment factors for the bystander and trunk mount antennas

Frequency, MHz	1-g SAR factors	10-g SAR factors
30	1.0	1.0
50	1.0	1.0
75	1.0	1.1
100	1.4	1.3
150	1.3	1.3
300	1.6	1.6
450	1.5	1.8
800	1.3	2.3
1000	1.1	2.5

Table VI: Whole-body average SAR adjustment factors for the passenger and roof mount antennas

Frequency, MHz	Centre roof mount antenna			Side roof mount antenna		
	Passenger location in the vehicle					
	Back seat, centre	Back seat, side	Front seat	Back seat, centre	Back seat, side	Front seat
33	1.8	1.0	1.3	1.4	1.1	1.3
80	1.0	1.3	8.2	1.0	1.4	8.3
150	1.9	2.4	1.6	2.0	1.5	1.7
450	1.8	2.9	2.5	4.7	2.7	1.8
800	2.7	2.1	2.2	2.7	2.3	2.8
1000	2.8	2.4	2.3	5.7	3.1	2.7

Table VII: Whole-body average SAR adjustment factors for the passenger and roof mount antennas

Frequency, MHz	Centre roof mount antenna						Side roof mount antenna					
	Back seat, centre		Back seat, side		Front seat		Back seat, centre		Back seat, side		Front seat	
	1-g	10-g	1-g	10-g	1-g	10-g	1-g	10-g	1-g	10-g	1-g	10-g
33	1.1	1.1	1.0	1.0	1.0	1.0	1.0	1.0	1.0	1.0	1.0	1.0
80	1.0	1.0	1.3	1.4	5.8	6.5	1.0	1.0	1.0	1.0	6.3	6.1
150	1.3	1.1	1.0	1.0	1.0	1.1	1.2	1.0	1.0	1.0	1.9	1.8
450	2.6	2.3	1.7	1.4	2.3	2.6	3.9	3.8	1.8	2.3	1.0	1.0
800	2.7	2.7	1.6	1.8	1.0	1.0	2.6	2.2	1.9	1.5	2.0	1.5
1000	2.2	2.3	1.4	1.4	1.7	2.1	5.6	4.8	2.5	3.1	1.3	1.5

Table VIII: Adjusted SAR Results

Mount location	Antenna Kit #	Freq [MHz]	Exposure location	Computation SAR [W/kg]			Interpolated Adjustment Factors			Adjusted SAR Results [W/kg]		
				1-g	10-g	WB	1-g	10-g	WB	1-g	10-g	WB
Trunk	HAD4022A (132-174MHz)	143.9875	Back Center	0.443	0.282	0.0184	1.82	1.91	2.31	0.81	0.54	0.042
			Back Side	0.157	0.104	0.0112	3.93	4.11	2.83	0.62	0.43	0.032
		150.8	Back Center	0.286	0.177	0.0127	1.90	2	2.40	0.54	0.35	0.030
			Back Side	0.147	0.077	0.0080	4.19	4.39	3.00	0.62	0.34	0.024
		158.3	Back Center	0.335	0.201	0.0147	1.91	2.01	2.41	0.64	0.40	0.035
			Back Side	0.224	0.157	0.0121	4.14	4.34	2.99	0.93	0.68	0.036
		165.9875	Back Center	0.398	0.246	0.0162	1.93	2.02	2.42	0.77	0.50	0.039
			Back Side	0.251	0.225	0.0115	4.08	4.29	2.98	1.02	0.97	0.034
		173.4	Back Center	0.380	0.234	0.0171	1.94	2.03	2.43	0.74	0.47	0.042
			Back Side	0.306	0.191	0.0136	4.03	4.24	2.97	**1.23**	0.81	0.040
			Bystander 0 deg Front	0.156	0.101	0.0088	1.35	1.35	1.97	0.21	0.14	0.017
			Bystander 0 deg Rear	0.277	0.144	0.0067	1.35	1.35	1.97	0.37	0.19	0.013
			Bystander 45 deg Front	0.299	0.166	0.0094	1.35	1.35	2.01	0.40	0.22	0.019
			Bystander 45 deg Rear	0.310	0.180	0.0088	1.35	1.35	2.01	0.42	0.24	0.018
			Bystander 90 deg Front	0.316	0.203	0.0136	1.35	1.35	2.26	0.43	0.27	0.031
			Bystander 90 deg Rear	0.594	0.309	0.0141	1.35	1.35	2.26	0.80	0.42	0.032
Roof	HAD4006A (136-144MHz)	140.0125	Back Center	0.484	0.312	0.0197	1.77	1.86	2.26	0.86	0.58	0.045
			Back Side	0.325	0.188	0.0179	3.74	3.91	2.71	1.21	0.73	0.049
Roof	RAD4226A (136-144MHz)	140.0125	Back Center	0.480	0.309	0.0195	1.77	1.86	2.26	0.85	0.58	0.044
			Back Side	0.319	0.184	0.0175	3.74	3.91	2.71	1.19	0.72	0.047

The SAR distribution in the exposure condition that gave highest adjusted 1-g SAR is reported in Figure 4 (173.4 MHz, passenger on the side of the back seat, HAD4022A antenna).

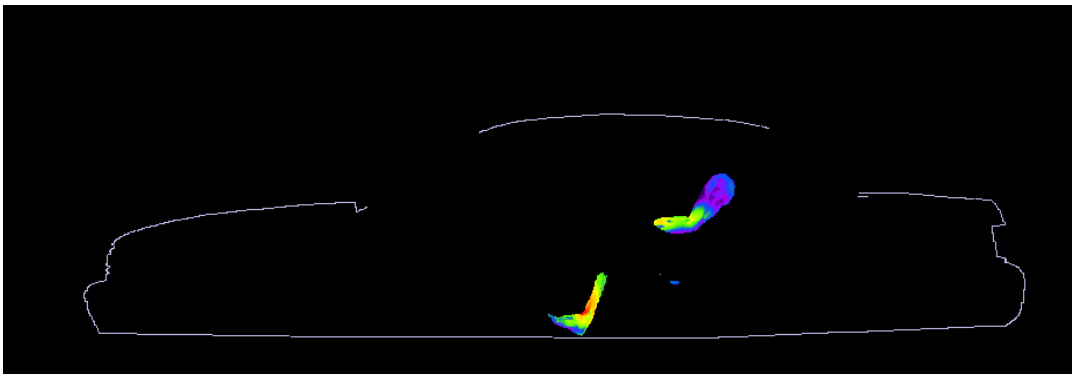

Figure 4. SAR distribution at 173.4 MHz in the passenger model located on the side of the back seat, produced by the trunk-mount HAD4022A antenna. The contour plot is relative to the plane where the peak 1-g average SAR for this exposure condition occurs.

The two pictures below in Figure 5 show the E and H field distributions in the plane of the antenna corresponding to the condition in Figure 3.

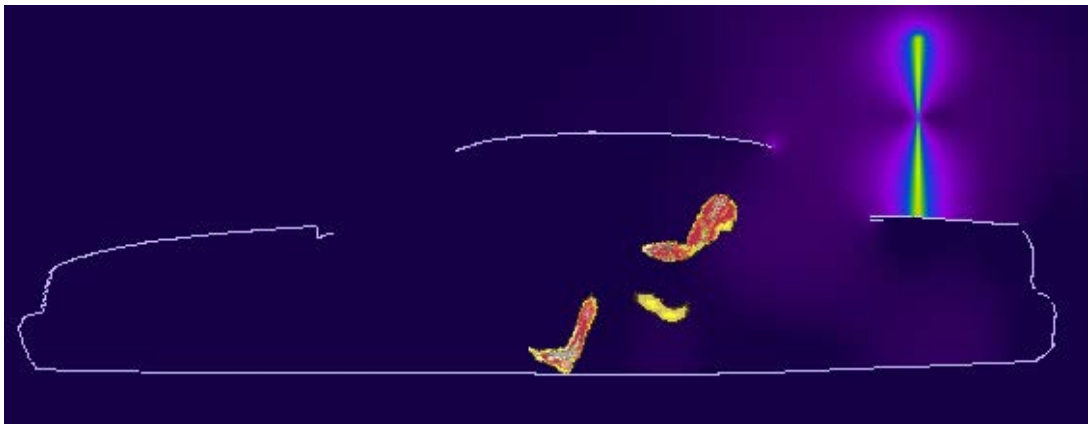

a)

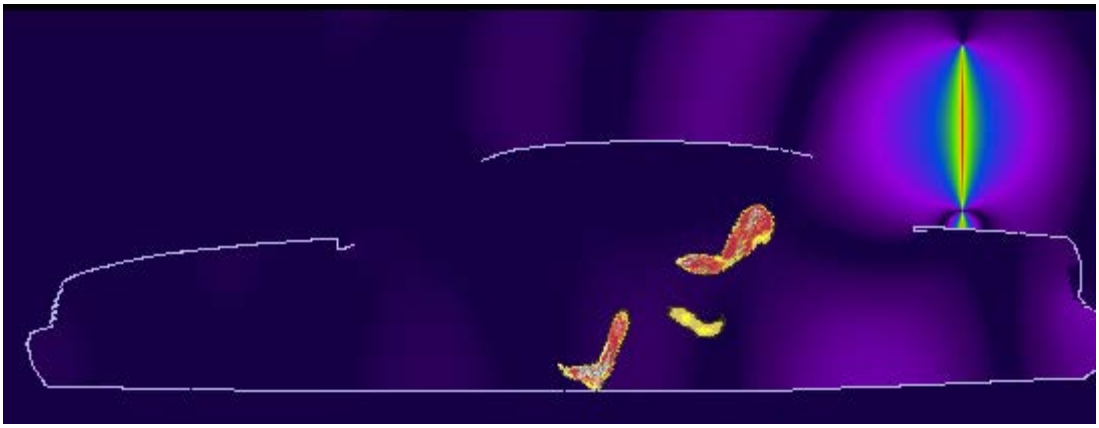

b)

Figure 4. (a) E-field distribution corresponding to exposure condition of Figure 3, and (b) H-field distribution corresponding to exposure condition of Figure 4.

The highest adjusted 1-g SAR was produced in the passenger exposure condition with HAD4022A antenna at 173.4 MHz (passenger on the side of the back seat).

Results of SAR Computations

The overall maximum peak 1-g SAR in all simulated conditions adjusted using the draft IEC/IEEE 62704-2 standard adjustment factor is 1.23 W/kg, less than the 1.6 W/kg limit, while the overall adjusted maximum peak 10-g SAR is 0.97 W/kg, less than the 2.0 W/kg limit. The adjusted maximum whole-body average SAR is 0.049 W/kg, less than the 0.08 W/kg limit.

Conclusions

Under the test conditions described for evaluating passenger exposure to the RF electromagnetic fields emitted by vehicle-mounted antennas used in conjunction with this mobile radio product, the present analysis shows that the computed SAR values are compliant with the FCC and Industry Canada exposure limits for the general public as well as with the corresponding ICNIRP and IEEE Std. C95.1-2005 SAR limits.

References

[1] IEEE Standard C95.1-1999. *IEEE Standard for Safety Levels with Respect to Human Exposure to RF Electromagnetic Fields*, 3 kHz to 300 GHz.

[2] http://www.nlm.nih.gov/research/visible/visible_human.html

[3] ICNIRP (International Commission on Non-Ionising Radiation Protection). 1998. *Guidelines for limiting exposure to time-varying electric, magnetic and electromagnetic fields (up to 300 GHz)*. Health Phys. 74:494–522.

[4] IEEE. 2005. *IEEE standard for safety levels with respect to human exposure to radio frequency electromagnetic fields, 3 kHz to 300 GHz*, IEEE Std C95.1-2005

[5] Simon,W., Bit-Babik, G., "Effect of the variation in population on the whole-body average 1379 SAR of persons exposed to vehicle mounted antennas W. Simon", ICEAA September 2-7, 2012, Cape 1380 Town.

APPENDIX: SPECIFIC INFORMATION FOR SAR COMPUTATIONS

This appendix follows the structure outlined in Appendix B.III of the Supplement C to the FCC OET Bulletin 65. Most of the information regarding the code employed to perform the numerical computations has been adapted from the draft IEC/IEEE 62704-1 and 62704-2 standards, and from the XFDTD™ User Manuals. Remcom Inc., owner of XFDTD™, is kindly acknowledged for the help provided.

1) Computational resources

a) A multiprocessor system equipped with two Intel Xeon X5570 quad-core CPUs and four Tesla C1060 GPUs was employed for all simulations.

b) The memory requirement was from 7 GB to 12 GB. Using the above-mentioned system with 8-cores operating concurrently, the typical simulation would run for 6-10 hours and with all four GPUs activated by the XFDTD version 7.3 this time would be from 60-180 min.

2) FDTD algorithm implementation and validation

a) We employed a commercial code (XFDTD™ v7.2, by Remcom Inc.) that implements the Yee's FDTD formulation [1]. The solution domain was discretized according to a rectangular grid with an adaptive 3-10 mm step in all directions. Sub-gridding was not used. Seven-layer PML absorbing boundary conditions are set at the domain boundary to simulate free space radiation processes. The excitation is a lumped voltage generator with 50-ohm source impedance. The code allows selecting *wire objects* without specifying their radius. We used a wire to represent the antenna. The car body is modeled by solid metal. We did not employ the "thin wire" algorithm since within the adaptive grid the minimum resolution of 3 mm was specified and used to model the antenna and the antenna wire radius was never smaller than one-fifth of the voxel dimension. In fact, the XFDTD™ manual specifies that "In most cases, standard PEC material will serve well as a wire. However, in cases where the wire radius is important to the calculation and is less than 1/4 the length of the average cell edge, the thin wire material may be used to accurately simulate the correct wire diameter." The maximum voxel dimension in the plane normal to the antenna in all our simulations was 3 mm, and the antenna radius is always at least 1 mm (1 mm for the short quarter-wave antennas and 1.5 mm for the long gain antennas), so there was no need to specify a "thin wire" material.

Because the field impinges on the bystander or passenger model at a distance of several tens of voxels from the antenna, the details of antenna wire modeling are not expected to have significant impact on the exposure level.

b) XFDTD™ is one of the most widely employed commercial codes for electromagnetic simulations. It has gone through extensive validation and has proven its accuracy over time in many different applications. One example is provided in [3].

We carried out a validation of the code algorithm by running the canonical test case involving a half-wave wire dipole. The dipole is 0.475 times the free space wavelength at 160 MHz, i.e.,

88.5 cm long. The discretization used to model the dipole was 5 mm. Also in this case, the “thin wire” model was not needed. The following picture shows XFDTD™ outputs regarding the antenna feed-point impedance (70.5 – j 6.0 ohm), as well as qualitative distributions of the total E and H fields near the dipole. The radiation pattern is shown as well (one lobe in elevation). As expected, the 3 dB beamwidth is about 78 degrees.

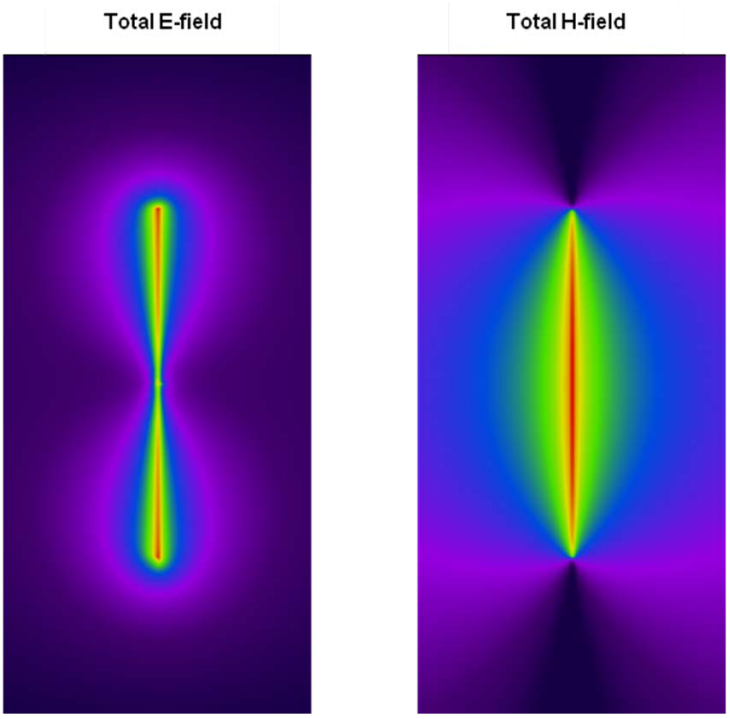

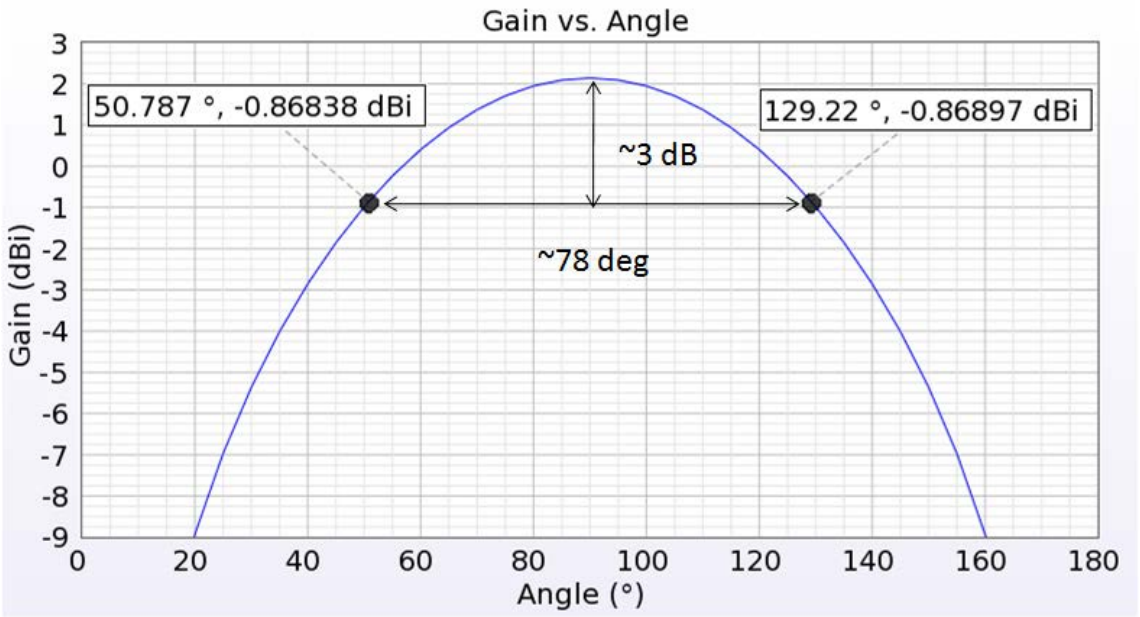

We also compared the XFDTD™ result with the results derived from NEC [4], which is a code based on the method of moments. In this case, we used a dipole with radius 1 mm, length 88.5 cm, and the discretization is 5 mm. The corresponding input impedance at 160 MHz is 69.5-j10.5 ohm. Its frequency dependence is reported in the following figure.

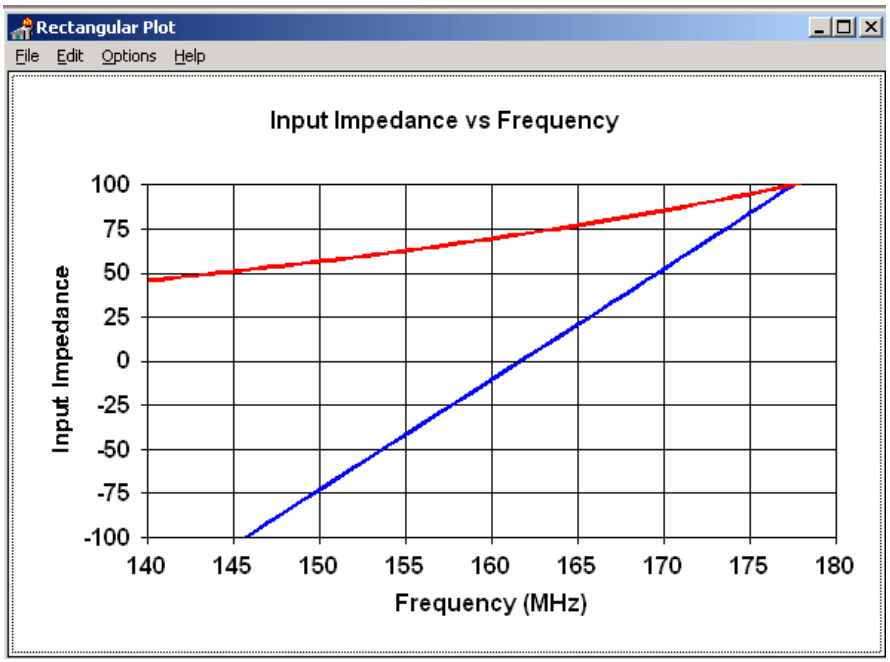

This validation ensures that the input impedance calculation is carried out correctly in XFDTD™, thereby enabling accurate estimates of the radiated power. It further ensures that the wire model employed in XFDTD™, which we used to model the antennas, produces physically meaningful current and fields distributions. Both these aspects ensure that the field quantities are correctly computed both in terms of absolute amplitude and relative distribution.

3) Computational parameters

a) The following table reports the main parameters of the FDTD model employed to perform our computational analysis:

PARAMETER	X	Y	Z
Voxel size	3-9 mm	3-9 mm	1-9 mm
Maximum domain dimensions employed for passenger computations with the trunk-mount antennas	397	910	559
Maximum domain dimensions employed for bystander computations with the trunk-mount antennas	449	791	709
Time step	About 0.7 of the Courant limit (typically 5 *ps*)		
Objects separation from FDTD boundary (mm)	>200	>200	>200
Number of time steps	Enough to reach at least -60 dB convergence		
Excitation	Sinusoidal (not less than 10 periods)		

4) Phantom model implementation and validation

a) The human body models (bystander and/or passenger) employed in our simulations are those defined in the draft IEEE 62704-2 standard. They are originally based on data from the *visible human project* sponsored by the National Library of Medicine (NLM) (http://www.nlm.nih.gov/research/visible/visible_human.html). The original male data set consists of MRI, CT and anatomical images. Axial MRI images of the head and neck and longitudinal sections of the rest of the body are available at 4 mm intervals. The MRI images have 256 pixel by 256 pixel resolution. Each pixel has 12 bits of gray tone resolution. The CT data consists of axial CT scans of the entire body taken at 1 mm intervals at a resolution of 512 pixels by 512 pixels where each pixel is made up of 12 bits of gray tone. The axial anatomical images are 2048 pixels by 1216 pixels where each pixel is defined by 24 bits of color. The anatomical cross sections are also at 1 mm intervals and coincide with the CT axial images. There are 1871 cross sections. Dr. Michael Smith and Dr. Chris Collins of the Milton S. Hershey Medical Center, Hershey, Pa, created the High Fidelity Body mesh. Details of body model creation are given in the *methods* section in [5].

The final bystander and passenger model was generated for the IEEE 62704-2 standard from the above dataset using the Varipose softwar, Remocm Inc., The body mesh contains 39 tissues materials. Measured values for the tissue parameters for a broad frequency range are included with the mesh data. The correct values are interpolated from the table of measured data and entered into the appropriate mesh variables. The tissue conductivity and permittivity variation *vs.* frequency is included in the XFDTD™ calculation by a multiple-pole approximation to the Cole-Cole approximated tissue parameters reported in [11].

a) The XFDTD™ High Fidelity Body Mesh model correctly represents the anatomical structure and the dielectric properties of body tissues, so it is appropriate for determining the highest exposure expected for normal device operation.

b) One example of the accuracy of XFDTD™ for computing SAR has been provided in [6]. The study reported in [6] is relative to a large-scale benchmark of measurement and computational tools carried out within the IEEE Standards Coordinating Committee 34, Sub-Committee 2.

5) Tissue dielectric parameters

a) The following table reports the dielectric properties computed for the 39 body tissue materials in the employed human body models at 150 MHz.

#	Tissue	ε_r	σ (S/m)	Density (kg/m^3)
1	bile	85.3	1.60	928
2	body fluid	71.3	1.26	1050
3	eye cornea	69.0	1.07	1051
4	fat	12.2	0.07	911
5	lymph	65.7	0.81	1035
6	mucous membrane	59.2	0.56	1102
7	toe, finger, and nails	14.4	0.07	1908
8	nerve spine	42.3	0.36	1075
9	muscle	62.2	0.73	1090
10	heart	80.7	0.79	1081
11	white matter	50.3	0.35	1041
12	stomach	73.3	0.92	1088
13	glands	65.7	0.81	1028
14	blood vessel	54.0	0.49	1102
15	liver	61.7	0.53	1079
16	gall bladder	71.3	1.06	1071
17	spleen	78.8	0.86	1089
18	cerebellum	74.6	0.85	1045
19	cortical bone	14.4	0.07	1908
20	cartilage	51.4	0.50	1100
21	ligaments	50.8	0.50	1142
22	skin	61.5	0.54	1109
23	large intestine	73.8	0.72	1088
24	tooth	14.4	0.07	2180
25	grey_matter	70.1	0.60	1045
26	eye lens	41.7	0.32	1076
27	outer lung	61.9	0.59	1050
28	small intestine	83.4	1.72	1030
29	eye sclera	63.5	0.93	1032
30	inner lung	28.3	0.32	394
31	pancreas	65.7	0.81	1087
32	blood	71.3	1.26	1050
33	cerebro_spinal_fluid	81.2	2.16	1007
34	eye vitreoushumor	69.1	1.51	1005
35	kidneys	85.0	0.88	1066
36	bone marrow	13.2	0.16	1029
37	bladder	21.4	0.30	1086
38	testicles	70.3	0.94	1082
39	cancellous bone	25.5	0.19	1178

b) The tissue types and dielectric parameters used in the SAR computation are appropriate for determining the highest exposure expected for normal device operation, because they are derived from measurements performed on real biological tissues (XFDTD, Reference Manual Version 6.4, Remcom, Inc.).

c) The tabulated list of the dielectric parameters used in phantom models is provided at point 5(a). As regards the device (car plus antenna), we used perfect electric conductors.

6) Transmitter model implementation and validation

a) The essential features that must be modeled correctly for the particular test device model to be valid are:

- Car body. The car model is very similar to the car used for MPE measurements, so as to be able to correlate measured and simulated field values. This car model has been developed for the SAR computational draft standard IEC/IEEE 62704-2.
- Antenna. We used a straight wire, even when the gain antenna has a base coil for tuning. All the coil does is compensating for excess capacitance due to the antenna being slightly longer than half a wavelength. We do not need to do that in the model, as we used normalization with respect to the net radiated power, which is determined by the input resistance only. In this way, we neglect mismatch losses and artificially produce an overestimation of the SAR, thereby introducing a conservative bias in the model. This simulation model was also validated by comparing the computed and measured near-field distributions in the condition with antenna mounted on the reference ground plane and showed good agreement experimental data [9].
- Antenna location. We used the same location, relative to the edge of the car trunk, the backseat, or the roof, used in the MPE measurements. The following pictures show a lateral and a perspective view of the bystander and passenger model.

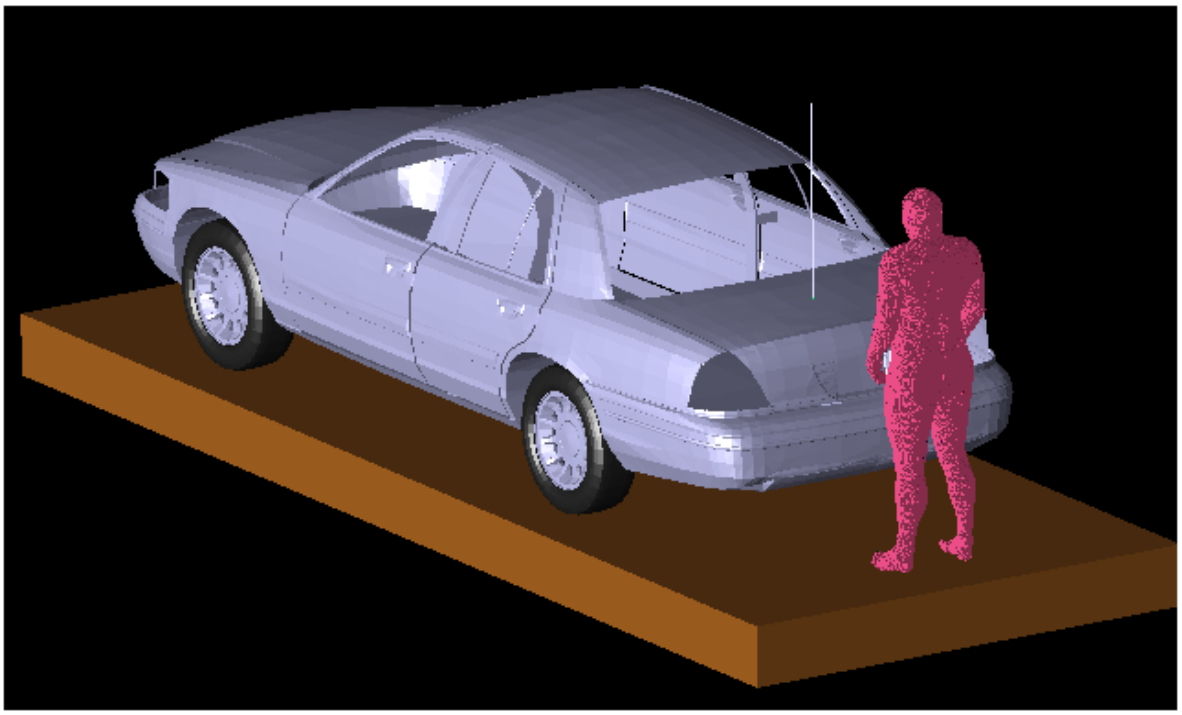

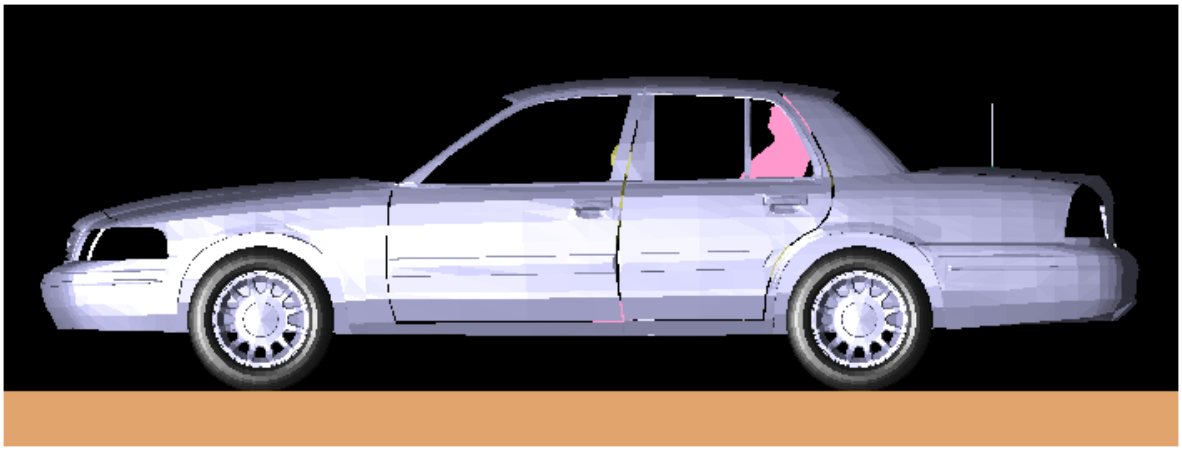

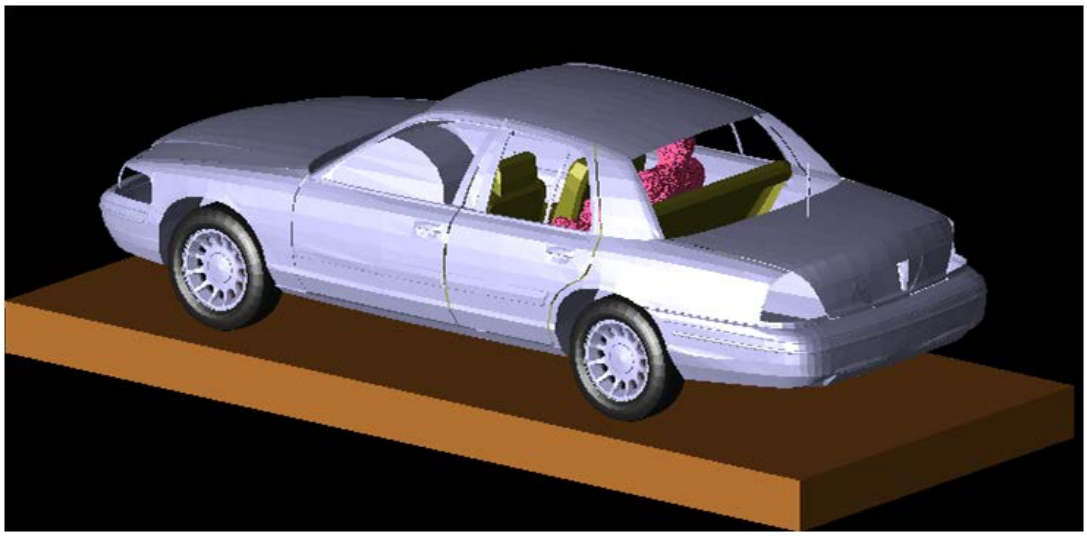

The car model is constituted by perfect electric conductor and does not include wheels in order to reduce its complexity. The passenger model is surrounded by air, as the seat, which is made out of poorly conductive fabrics, is not included in the computational model. The pavement has not been included in the model. The passenger and bystander models were validated for similar antenna and frequency conditions by comparing the MPE measurements at two VHF frequencies (146 MHz and 164 MHz) for antennas used for a VHF mobile radio analyzed previously in 2003 (FCC ID#ABZ99FT3046). The corresponding MPE measurements are reported in the compliance report relative to FCC ID#ABZ99FT3046. The comparison results are presented below, according to following definitions for the equivalent power densities (based on E or H-field):

$$S_E = \frac{|\mathbf{E}|^2}{2\eta}, \quad S_H = \frac{\eta}{2}|\mathbf{H}|^2, \quad \eta = 377\ \Omega$$

Passenger with 43 cm monopole antenna (HAD4009A 164 MHz)

The following figures of the test model show the empty car model, where the red dotted line represents the location of the passenger in the back seat, as it can be observed from the complete model picture above. The comparison has been performed by taking the computed steady-state field values at the red dots locations corresponding to the head, chest, and lower trunk area and comparing them with the corresponding measurements. Such a comparison is carried out at the same average power level (56.5 W) used in the measurements. Steady-state E-field and H-field distributions at a vertical crossing the passenger's head are displayed as well. Finally, a picture of the antenna is shown.

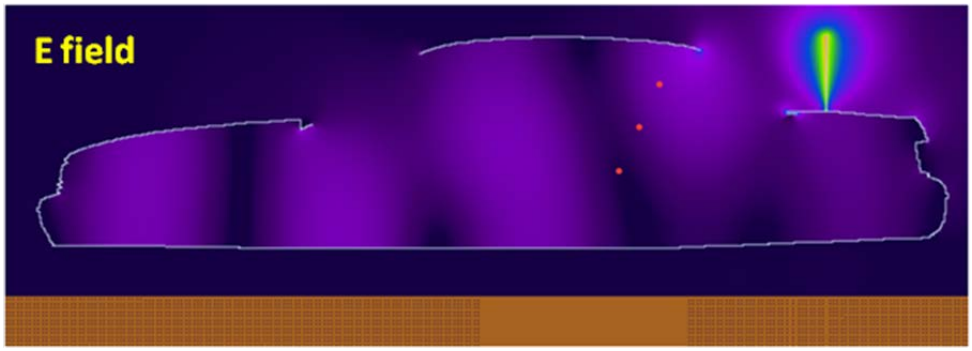

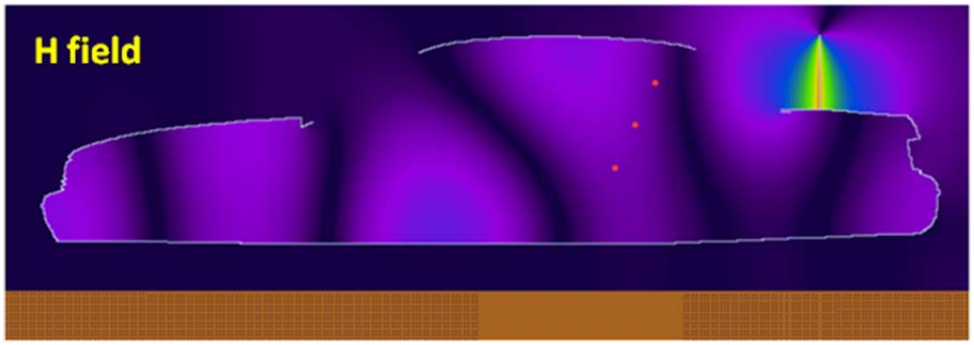

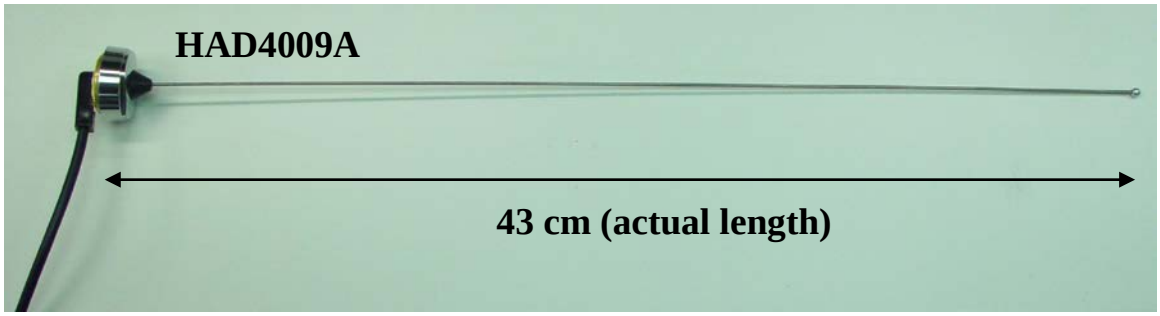

The highest exposure occurs in the middle of the backseat, which is also the case in the measurements. Therefore, the field values were determined on the yellow line centered at the middle of the backseat, approximately at the three locations that are shown by white dots. In actuality, the line is inclined so as to follow the inclination of the passenger's back, as shown previously.

Because the peak exposure occurs in the center of the back seat, that was where we placed the passenger model to perform the SAR evaluations presented in the report. However, it can be observed that the H-field distribution features peaks near the lateral edges of the rear window. That is the reason why we also carried out one SAR computation by placing the passenger laterally in the back seat, in order to determine whether the SAR would be higher in this case.

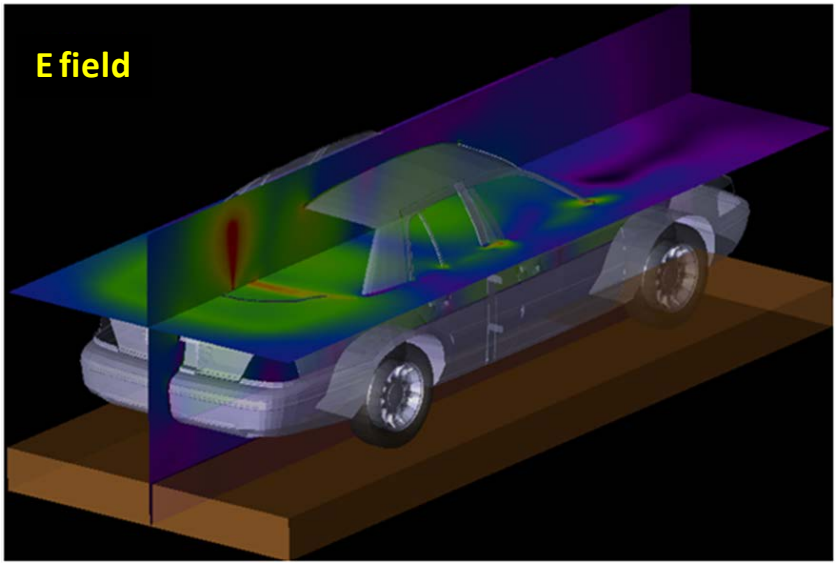

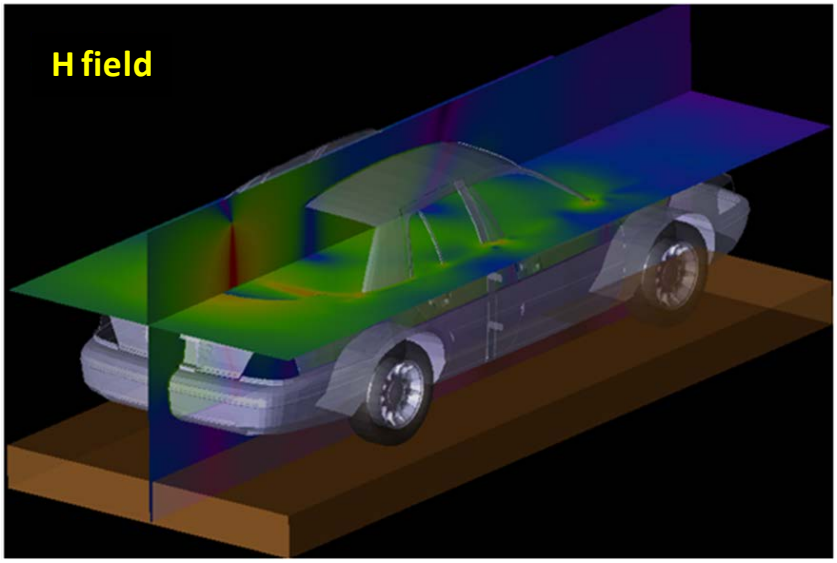

As done in the measurements, the equivalent power density (S) is computed from the E-field, the H-field being much lower. The following table reports the E-field values computed by XFDTD™ at the three locations, and the corresponding power density.

Location	E-field magnitude (V/m)	S (W/m^2)
Head	1.27	2.14E-03
Chest	0.70	6.55E-04
Lower Trunk area	0.20	7.70E-05
	Average S	**9.57E-04**

The input impedance is 24.8-j11.9 ohm, therefore the radiated power (considering the mismatch to the 50 ohm unitary voltage source) is 2.16E-3 W. The scaled-up power density for 56.5 W radiated power is 25.0 W/m^2, corresponding to 2.50 mW/cm^2. Measurements gave an average of

1.29 mW/cm^2, which is a reasonable overestimation considering conservativeness of simulations model. The following table and the graph show a comparison between the simulated power density and the measured one (see also MPE report in FCC ID#ABZ99FT3046, Table 43), normalized to 56.5 W radiated.

Position	SE (meas) mW/cm^2	SE (FDTD) mW/cm^2
Head	2.98	5.59
Chest	0.74	1.71
Lower Trunk	0.14	0.2

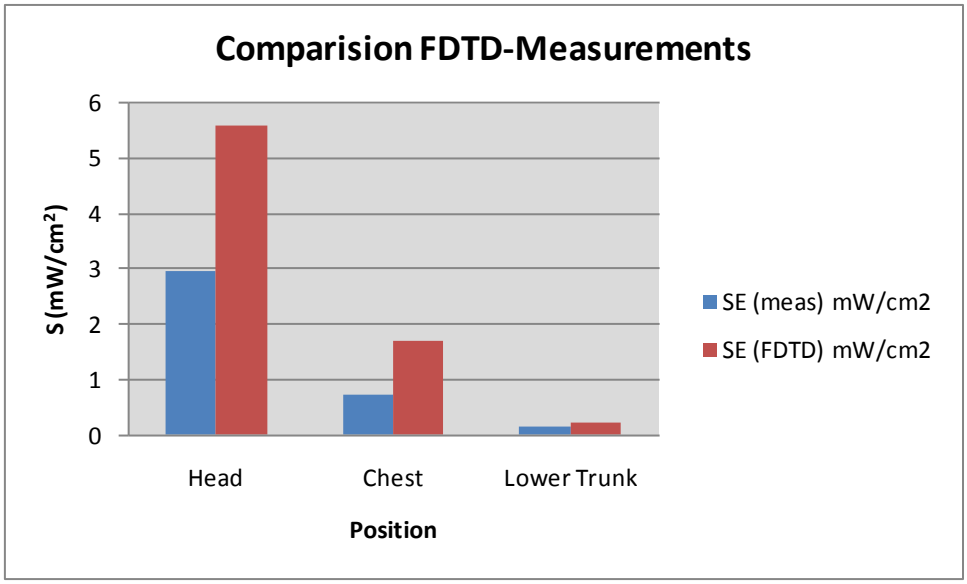

Bystander with 48 cm monopole antenna (HAD4007A 146 MHz)

The following figures show the E-field and H-field distributions across a vertical plane passing for the antenna and cutting the car in half. As done in the measurements, the MPE is computed from both E-field and H-field distributions, along the yellow dotted line at 10 points spaced 20 cm apart from each other up to 2 m in height. These lines and the field evaluation points are approximately indicated in the figures. The E-field and H-field distributions in the vertical plane placed at 60 cm from the antenna, are shown as well. The points where the fields are sampled to determine the equivalent power density (S) are approximately indicated by the white dots. A picture of the antenna is not reported because it is identical to the HAD4009A except for the length.


E field
60 cm
(0 mm, 200 mm, 0 mm)


H field
60 cm
(0 mm, 200 mm, 0 mm)

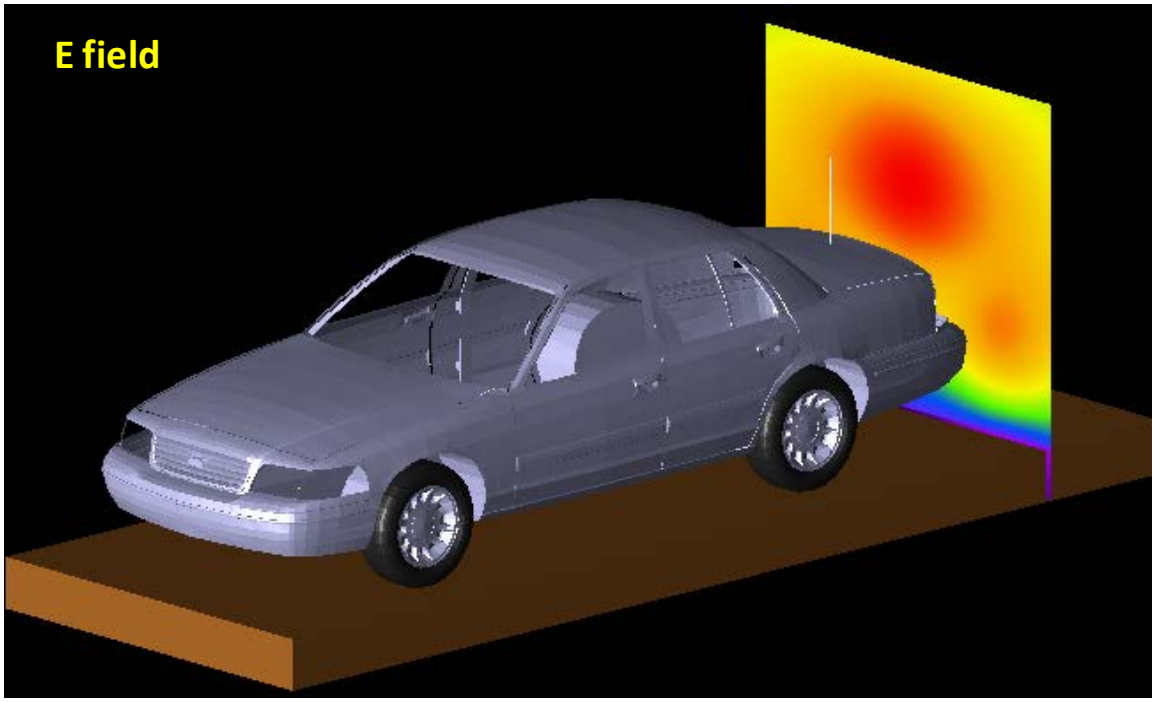
E field

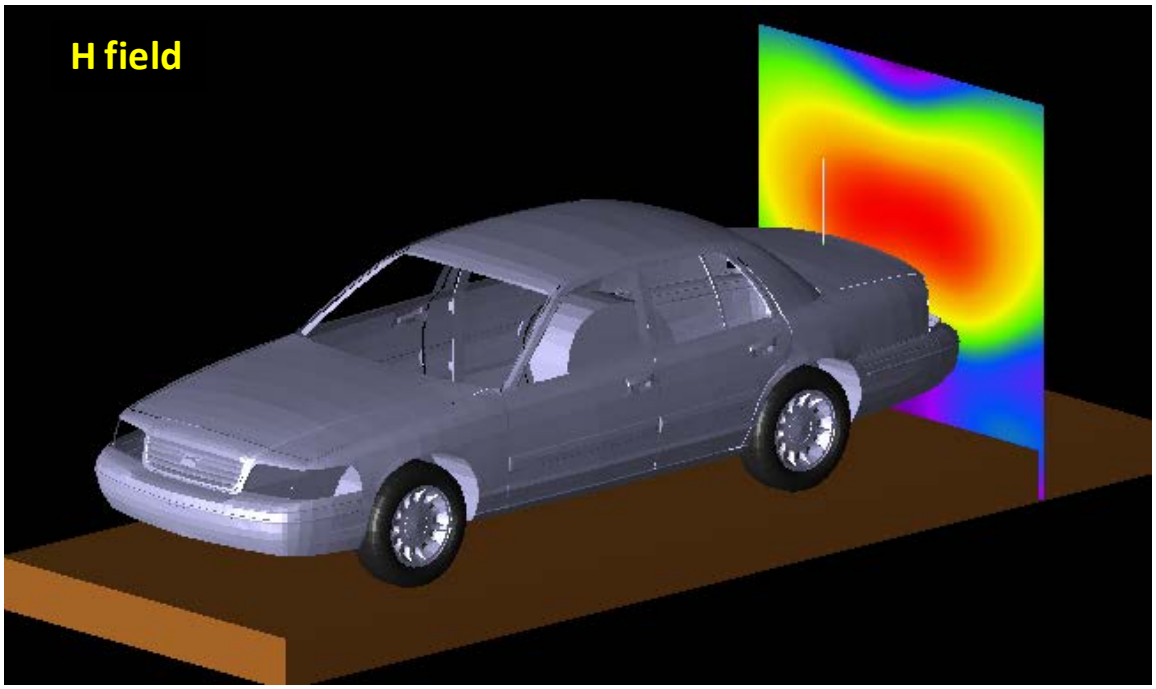

The following table reports the field values computed by XFDTD™ and the corresponding power density values. The average exposure levels are computed as well.

Height (cm)	E (V/m)	S_E (W/m^2)	H (A/m)	S_H (W/m^2)
20	1.84E-01	4.50E-05	5.10E-04	4.89E-05
40	2.71E-01	9.71E-05	6.38E-04	7.68E-05
60	3.58E-01	1.70E-04	1.08E-03	2.20E-04
80	4.42E-01	2.59E-04	1.54E-03	2.20E-04
100	5.85E-01	4.55E-04	1.82E-03	4.48E-04
120	6.86E-01	6.24E-04	1.85E-03	6.23E-04
140	6.82E-01	6.17E-04	1.58E-03	6.42E-04
160	5.93E-01	4.67E-04	1.16E-03	4.72E-04
180	4.63E-01	2.84E-04	7.67E-04	2.52E-04
200	3.41E-01	1.55E-04	4.94E-04	1.11E-04
	Average S_E	**3.17E-04**	**Average S_H**	**3.11E-04**

The input impedance is 33.7-j3.0 ohm, therefore the radiated power (considering the mismatch to the 50 ohm unitary voltage source) is 2.40E-3 W. The scaled-up power density values for 53.2 W radiated power are 7.03 W/m^2 (E), and 6.90 W/m^2 (H), that correspond to 0.70 mW/cm^2 (E), and 0.69 mW/cm^2 (H). Measurements yielded average power density of 0.664 mW/cm^2 (E), and 0.471 mW/cm^2 (H), i.e., which are in good agreement with the simulations. The following table and graph show a comparison between the simulated power density and the measured one, based on E (see MPE report in FCC ID#ABZ99FT3046, Table 1) or H fields (see MPE report in FCC ID#ABZ99FT3046, Table 13), normalized to 53.2 W radiated.

Height (cm)	SE (meas) mW/cm^2	SE (FDTD) mW/cm^2	SH (meas) mW/cm^2	SH (FDTD) mW/cm^2	Avg SE meas mW/cm^2	Avg SE FDTD mW/cm^2	Avg SH meas mW/cm^2	Avg SH FDTD mW/cm^2
20	0.19	0.10	0.2	0.11	0.664	0.703	0.471	0.690
40	0.37	0.22	0.23	0.17				
60	0.55	0.38	0.3	0.49				
80	0.68	0.57	0.56	0.49				
100	1.02	1.01	1.07	0.99				
120	1.15	1.38	1.1	1.38				
140	1.04	1.37	0.56	1.42				
160	0.79	1.03	0.24	1.05				
180	0.5	0.63	0.23	0.56				
200	0.35	0.34	0.22	0.25				

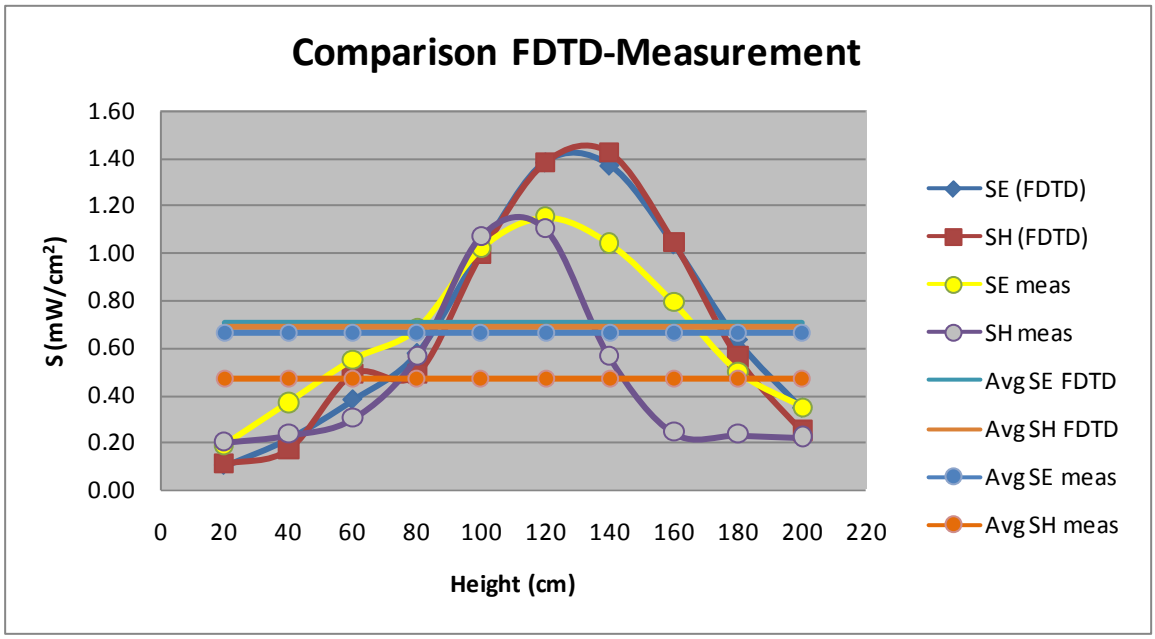

7) Test device positioning

a) A description of the device test positions used in the SAR computations is provided in the SAR report.

b) Illustrations showing the separation distances between the test device and the phantom for the tested configurations are provided in the SAR report.

8) Steady state termination procedures

a) The criteria used to determine that sinusoidal steady-state conditions have been reached throughout the computational domain for terminating the computations are based on the monitoring of field points to make sure they converge. The simulation projects were set to automatically track the field values throughout computational domain by means of XFDTD simulation control feature which ensures that "*convergence is reached when near-zone data shows a constant amplitude sine wave – when all transients have died down and the only variation left is sinusoidal. In this case "convergence" is tested on the average electric field in the space for its deviation from a pure sine wave. XFDTD automatically places points throughout the space for this purpose.*" [XFDTD Reference Manual, version. 6.4 and version 7.2]. This convergence threshold was set to -50 dB.
In addition for at least one passenger and one bystander exposure condition, we placed one "field sensor" near the antenna, others between the body and the domain boundary at different locations, and one inside the head of the model. In all simulations, isotropic E-field sensors were placed at opposite sides of the computational domain. We used isotropic E and H field "sensors", meaning that all three components of the fields are monitored at these points. The following figures show an example of the time waveforms at the field point sensors in two points of the computational domain. We selected points close to antenna as well as furthest one. The highest field levels are observed for the higher index point, as it is closer to the antenna. In all cases, the field reaches the steady-state condition.

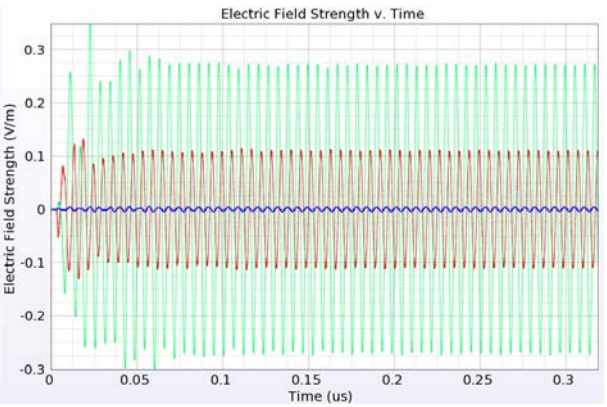

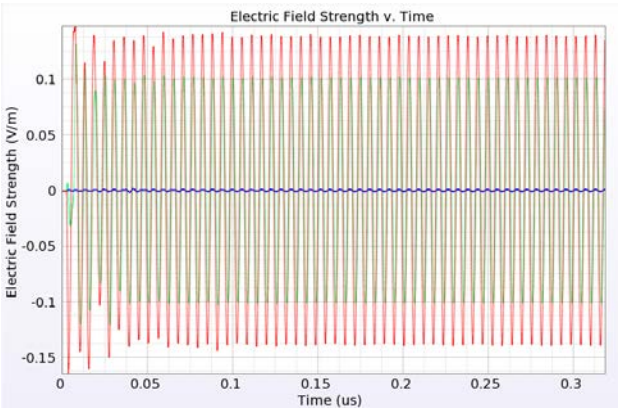

c) The XFDTD™ algorithm determines the field phasors by using the so-called "two-equations two-unknowns" method. Details of the algorithm are explained in [7].

9) Computing peak SAR from field components

a) The SAR for an individual voxel is computed according to the draft IEEE 62704-1 standard. In particular, the three components of the electric field are computed in the center of each voxel and then the SAR is computed as below:

$$SAR = \sigma_{voxel} \frac{|E_x|^2 + |E_y|^2 + |E_z|^2}{2\rho_{voxel}},$$

where σ_{voxel} and ρ_{voxel} are the conductivity and the mass density of the voxel.

10) One-gram and ten-gram averaged SAR procedures

a) XFDTD™ computes the Specific Absorption Rate (SAR) in each complete cell containing lossy dielectric material and with a non-zero material density. Using the SAR values computed for each voxel of the model the averaging calculation employs the method and specifications defined in the draft IEEE 62704-1 standard to generate one-gram and ten-gram average SAR.

11) Total computational uncertainty – We derived an estimate for the uncertainty of FDTD methods in evaluating SAR by referring to [6]. In Fig. 7 in [6] it is shown that the deviation between SAR estimates using the XFDTD™ code and those measured with a compliance system are typically within 10% when the probe is away from the phantom surface so that boundary effects are negligible. In that example, the simulated SAR always exceeds the measured SAR.

As discussed in 6(a), a conservative bias has been introduced in the model so as to reduce concerns regarding the computational uncertainty related to the car modeling, antenna modeling, and phantom modeling. The results of the comparison between measurements and simulations presented in 6(a) suggest that the present model produces an overestimate of the exposure between 4% and 36%. Such a conservative bias should eliminate the need for including uncertainty considerations in the SAR assessment.

12) Test results for determining SAR compliance

a) Illustrations showing the SAR distribution of dominant peak locations produced by the test transmitter, with respect to the phantom and test device, are provided in the SAR report.

b) The input impedance and the total power radiated under the impedance match conditions that occur at the test frequency are provided by XFDTD™. XFDTD™ computes the input impedance by following the method outlined in [8], which consists in performing the integration of the steady-state magnetic field around the feed point edge to compute the steady-state feed point current (*I*), which is then used to divide the feed-gap steady-state voltage (*V*). The net average radiated power is computed as

$$P_{XFDTD} = \frac{1}{2}\mathrm{Re}\left\{VI^{*}\right\}$$

Both the input impedance and the net average radiated power are provided by XFDTD™ at the end of each individual simulation.

We normalize the SAR to such a power, thereby obtaining SAR per radiated Watt (*normalized SAR*) values for the whole body and the 1-g SAR. Finally, we multiply such normalized SAR values times the max power rating of the device under test. In this way, we obtain the exposure metrics for 100% talk-time, i.e., without applying source-based time averaging.

c) For mobile radios, 50% source-based time averaging is applied by multiplying the SAR values determined at point 12(b) times a 0.5 factor.

REFERENCES

[1] K. S. Yee, “Numerical Solution of Initial Boundary Value Problems Involving Maxwell's Equations in Isotropic Media,” *IEEE Transactions on Antennas and Propagation*, vol. 14, no. 3, 302-307, March 1966.

[2] Z. P. Liao, H. L. Wong, G. P. Yang, and Y. F. Yuan, "A transmitting boundary for transient wave analysis," Scientia Sinica, vol. 28, no. 10, pp 1063-1076, Oct. 1984.

[3] Validation exercise: Mie sphere. Remcom Inc. (enclosed PDF)

Remcom.pdf

[4] NEC-Win PRO ™ v 1.1, Nittany Scientific, Inc., Riverton, UT.

[5] C. M. Collins and M. B. Smith, "Calculations of B1 distribution, SNR, and SAR for a surface coil against an anatomically-accurate human body model," *Magn. Reson. Med.*, 45:692-699, 2001. (enclosed TIF)

Collins & Smith.pdf

[6] Martin Siegbahn and Christer Törnevik, “Measurements and FDTD Computations of the IEEE SCC 34 Spherical Bowl and Dipole Antenna,” Report to the IEEE Standards Coordinating Committee 34, Sub-Committee 2, 1998. (enclosed PDF)

Ericsson.pdf

[7] C. M. Furse and O. P. Gandhi, “Calculation of electric fields and currents induced in a millimeter-resolution human model at 60 Hz using the FDTD method with a novel time-to-frequency-domain conversion**,”** Antennas and Propagation Society International Symposium, 1996. (enclosed PDF)

Furse & Gandhi.pdf

[8] *The Finite Difference Time Domain Method for Electromagnetics*, Chapter 14.2, by K. S. Kunz and R. J. Luebbers, CRC Press, Boca Raton, Florida, 1993.

[9] *Validation of Mobile Antenna Modeling by Comparison with Near-field Measurements*," Report to the IEEE Standards Coordinating Committee 34, Sub-Committee 2, 2006. (enclosed PDF)

IEEE1528_2_vld.pdf

[10] *Antenna Theory: analysis and design*, Chapter 4, by C. A. Balanis, 2nd ed. John Wiley & Sons, Inc.

[11] S. Gabriel, R. W. Lau, and C. Gabriel. 1996. The dielectric properties of biological tissues: III. Parametric models for the frequency spectrum of tissues. Phys. Med. Biol. 41:2271–2293.